ABLATION, MELTING, AND SMOOTHING OF POLYCRYSTALLINE ALUMINA BY PULSED EXCIMER LASER RADIATION

Douglas H. Lowndes,* M. DeSilva,** M. J. Godbole,** A. J. Pedraza,** and D. B. Geohegan*
* Solid State Division, Oak Ridge National Laboratory, P. O. Box 2008,
Oak Ridge, TN 37831–6056
** Department of Materials Science and Engineering, The University of Tennessee,
Knoxville, TN 37996–2200

ABSTRACT

The effects of pulsed XeCl (308 nm) laser radiation on polycrystalline Al_2O_3 (alumina, 99.6% pure) and single-crystal Al_2O_3 (sapphire) are studied as a function of laser fluence. No laser etching of either material is detected below a threshold fluence value, which is much lower for alumina than for sapphire. Above this threshold, laser etching of both materials is observed following a number of incubation (induction) pulses. This number is much larger for sapphire than for alumina but decreases with increasing fluence for both materials. Laser etching rates for the two materials are similar at high fluences and after the incubation period. Scanning electron microscope images show that alumina melts and flows under repeated irradiation at fluences ≥0.7 J/cm^2. Atomic force microscopy and surface profilometry reveal significant smoothing of the as-received polycrystalline alumina surface after repeated irradiations at moderate fluences (~1–3 J/cm^2). Ion probe measurements for alumina in vacuum confirm the incubation behavior, and reveal that at fixed fluence the (positive) charge collected per pulse saturates after a sufficient number of pulses, as does the etch-plume velocity. The results are interpreted in terms of laser-generation of a sufficient concentration of absorption centers before efficient ablation/etching of these wide bandgap materials can occur.

INTRODUCTION

Extensive studies have been carried out of the mechanism for laser etching of sapphire (single crystal Al_2O_3, c-Al_2O_3) [1–6]. These studies were motivated by the fact that although sapphire has a low vapor pressure and wide energy bandgap, E_g ~9 eV, it nevertheless is easily etched using relatively low fluences of ultraviolet (UV) photons with energies of 5–6.3 eV, much less than E_g. Early studies showed that the threshold fluence for laser sputtering of sapphire coincided with the onset of intense emission from excited neutral Al atoms in the etch plume [1]. However, in regions of uniform laser irradiation there was no evidence of thermal melting, thermal-stress-induced fracture, or exfoliational processes, which suggested an electronic sputtering mechanism instead. Subsequent studies using a pulsed photothermal deformation (PPTD) technique revealed a large (~3%) absorption of laser energy at the (front and back) sapphire surfaces, and that this absorption is independent of laser fluence, thus ruling out the possibility that a multiphoton absorption process is responsible for laser etching of sapphire [5]. The fraction of energy absorbed at 193 nm, 248 nm, or 351 nm was independent of laser fluence for power densities below the ablation threshold, indicating a primarily one-photon absorption process. Chemical etching of the as-received (mechanically polished) sapphire surface greatly reduced the energy absorbed, proving that the PPTD signal comes from absorption sites located near the surfaces. Recent measurements using reflection electron-energy-loss spectroscopy (REELS) also revealed surface electronic states within the bulk bandgap of sapphire [6].

Dickinson and co-workers recently observed intense particle emission and surface etching when sodium trisilicate glass (STG, $Na_2O{\cdot}3\ SiO_2$) was irradiated by high-fluence (2.7–5 J/cm^2) pulsed KrF laser radiation (248 nm, 20 ns) [7, 8], but only *after an incubation period of several pulses*. At higher fluence, fewer incubation pulses were needed. Similar incubation behavior has been seen in pulsed laser ablation (PLA) of other materials [9–12]. They suggest that laser etching occurs only after an induction period because of the need to accumulate laser-generated absorption centers, which are then responsible for strong coupling of the laser pulse into the near-surface region, via single-photon excitation of electrons into the conduction band from mid-gap defect electronic levels, accompanied by rapid photon-heating of these "free electrons" [7]. More recently they *simultaneously* bombarded STG with 0.5–2.0 keV electrons and KrF laser pulses [13–15]. Laser etching of STG was initiated immediately, and could be sustained indefinitely at what had been sub-threshold laser fluences. They propose that near-surface

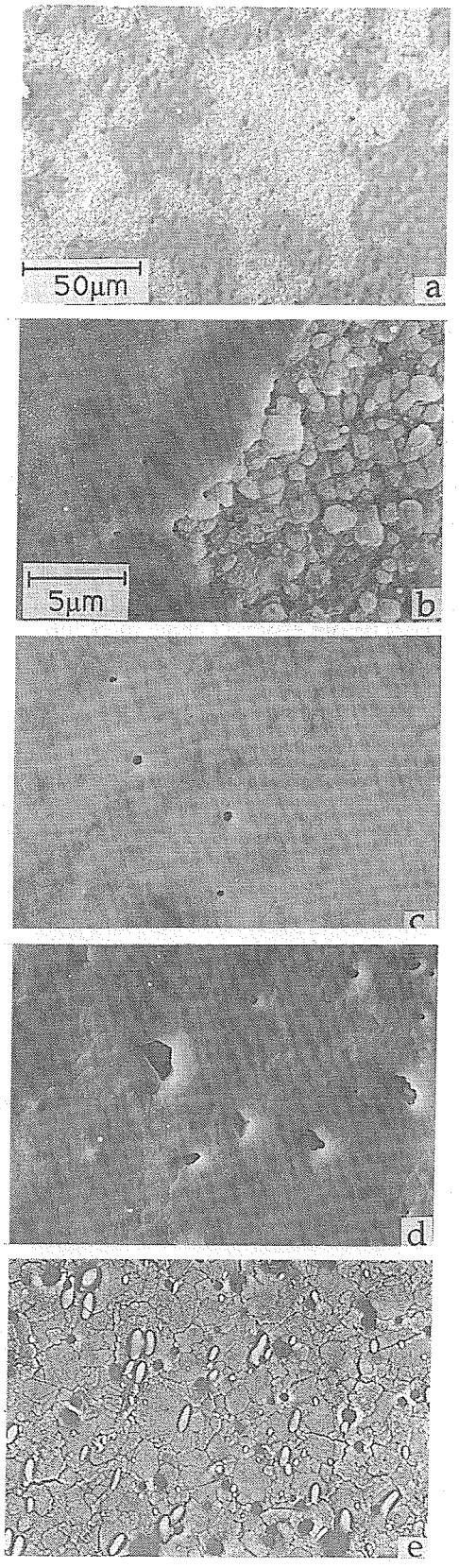

defects generated by inelastic scattering of the electron beam provide the single-photon absorption centers that facilitate laser etching. REELS measurements on electron-beam irradiated surfaces revealed mid-bandgap defect electronic states whose concentration increased with exposure [13].

The use of pulsed UV laser radiation to etch, micromachine, or alter surface chemical properties of wide bandgap materials is of obvious technological interest. The suggestion [7,13] that such changes can be brought about using easily controlled, single-photon processes, simply by introducing midgap electronic energy levels associated with near-surface defects, is especially attractive. In this paper we report results for laser etching of a technologically important material—polycrystalline alumina (p-Al_2O_3) thin-film substrates—and, for comparison, single-crystal sapphire. The alumina substrates contain a high concentration of native defects of a quite different type than those induced by electron– or laser–irradiation, namely grain boundaries and irregular crystalline facets on the micrometer scale.

EXPERIMENTAL

Polycrystalline alumina thin-film substrates having a uniform grain structure and surface finish were obtained from Coors Ceramics Co. (type ADS–996 "LustraSurf" thin-film substrates). These p-Al_2O_3 sheets are formed by a cast–tape process; the as–fired surface (cast on a polyester film) was used in our experiments. The p–Al_2O_3 purity is 99.6%, with MgO (0.17%) and SiO_2 (0.15%) the principal impurities. Scanning electron microscope (SEM) images [e.g. Fig. 1(b)] reveal individual grain diameters from 0.5 to nearly 3 μm, with most grains in the 1–2 μm range. The surface roughness was ~0.07–0.10 μm, as determined by a Dektak II surface profiler [but somewhat rougher as seen by the atomic force microscope, see Fig. 6(top)]. The effect of pulsed laser radiation on single-crystal sapphire also was studied using (2 $\bar{1}$ $\bar{1}$ 0)–oriented c-Al_2O_3 obtained from Saphikon. These samples (with dimensions 5 cm × 1.25 cm × 0.45 mm) had an 80/50 (scratch/dig) optical finish.

A pulsed XeCl (308 nm) excimer laser equipped with uniform–beam electrodes

Figure 1. SEM images of p–Al_2O_3 surfaces following 10 shots of pulsed XeCl laser radiation at (a) and (b) 0.7, (c) 1, (d) 3, and (e) 4 J/cm^2. The length scale is the same for (b)–(e).

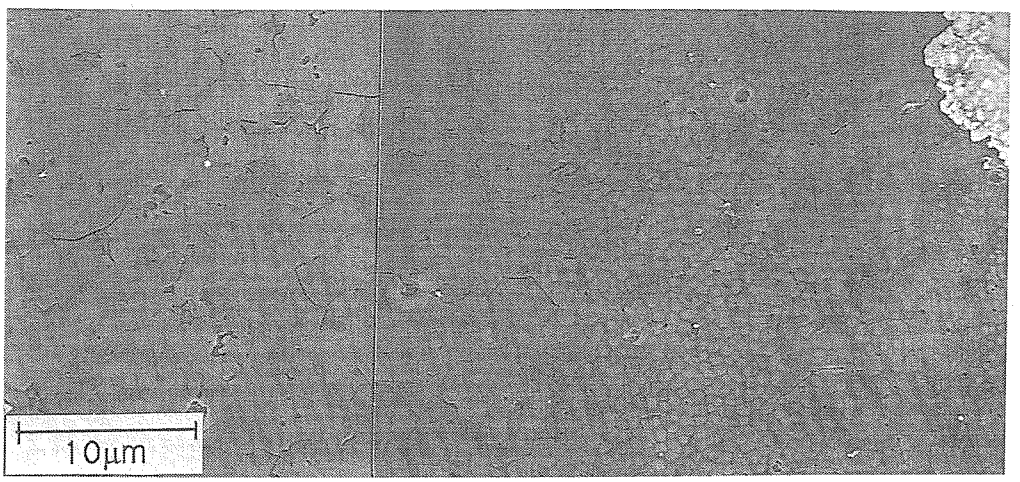

Figure 2. SEM image of the melted and resolidified sub-surface region of a p-Al_2O_3 sample following 10 pulses of XeCl radiation at 3 J/cm^2.

(FWHM pulse duration ~41 ns) was used for most of the irradiations of Al_2O_3 targets. The laser beam was passed through a rectangular aperture to remove its low energy density (E_d) fringe and was focused using a single f_L = 50 cm spherical lens. E_d was controlled by varying the lens–target separation. All XeCl irradiations were carried out in air. Studies of the formation and propagation of the plasma "plume"—generated by laser ablation of alumina in vacuum—were carried out using a pulsed KrF (248 nm) laser (FWHM pulse duration ~45 ns) and ion probe time–of–flight measurements. A few comparison measurements of the laser etch–depth for alumina in vacuum also were made using the KrF laser.

RESULTS

Figure 1 shows SEM images of the p–Al_2O_3 surface following irradiation in air by ten XeCl laser pulses at each of a series of increasing E_d values. The figure shows clearly that p–Al_2O_3 melts under these conditions, followed by flow and recrystallization. The melting threshold E_d value is ~0.7 J/cm^2, though melting is somewhat nonuniform [Fig. 1(a)] near threshold. At higher E_d values (1–3 J/cm^2), the flow of molten material resulting from ten laser shots produces a very smooth Al_2O_3 surface (as described below). For E_d = 4 J/cm^2, cracking of the recrystallized surface is evident, and the surface is covered by elongated frozen droplets of once–molten material that has been redeposited on the surface.

Computer model calculations of the heat flow during and immediately after absorption of the laser pulse were carried out, and showed that a melting threshold in the neighborhood of 1 J/cm^2 is reasonable from an energy balance point of view. However, the model calculations were highly idealized in not taking explicitly into account the very complex processes of Knudsen layer formation, laser energy absorption in the plasma and subsequent energy transfer from plasma to substrate, or the plasma's eventual free expansion [16,17].

In order to confirm melting and obtain information about the melt depth, p–Al_2O_3 specimens were irradiated with 10 shots at E_d = 1, 2, 3, 4, and 5 J/cm^2. Copper then was evaporated onto the surface except for a small circular opening and the samples were ion milled at 60° incidence angle through the opening. This created a slightly beveled surface (~1°–1.5° pitch), and exposed the sub-surface region to SEM examination. As illustrated in Fig. 2, cellular structure indicating melting and solidification was found to extend over a lateral distance > 30 μm in all of the beveled samples. This corresponds to a nearly constant (with E_d) thickness of 0.15–0.2 μm of once–molten material remaining behind. (The accuracy of this measurement is limited primarily by the ~0.07–0.10 μm roughness of the surrounding surface.) Taken together, the evidence of molten flow (Fig. 1), of a sub–surface cellular structure (Fig. 2), and of solidified droplets on the surface [Fig. 1(e)], all point toward the occurrence of thermal melting.

Progressive changes in the laser etch-depth and morphology of the laser–irradiated surface were studied as a function of E_d and the number of laser shots, using both Dektak II (mechanical

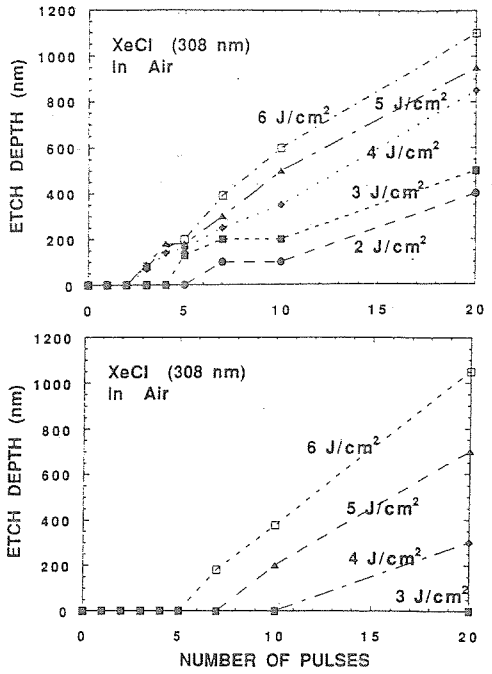

Figure 3. Dektak measurements of XeCl laser etch-depth vs number of shots for alumina (top) and for sapphire (bottom). The maximum depth of the etched crater is plotted.

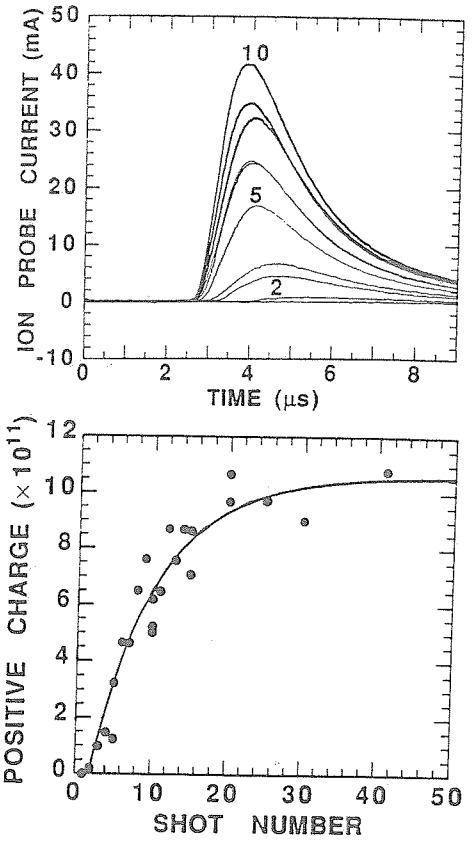

Figure 4. (Top) Ion probe waveforms for shots 1 through 10 at d = 8 cm from a p-Al_2O_3 target. (Bottom) Integrated area of the ion probe signal vs laser shot number (KrF laser, 1.1 J/cm^2).

stylus) and atomic force microscope (AFM) surface profile measurements. Figure 3 compares Dektak measurements of the laser etch–depth vs number of XeCl laser shots, for various E_d values, in both single–crystal and polycrystalline Al_2O_3. For these measurements, we define an etching threshold fluence, E_d^{thresh}, by the appearance of a laser-etched ("crater") region. The most striking differences between the c– and p–Al_2O_3 samples are their E_d^{thresh} values and the more pronounced incubation behavior before etching of sapphire occurs. For sapphire (Fig. 3, bottom), no etching was observed after 20 shots at 3 J/cm^2, and at 4 J/cm^2 the onset of significant laser etching came only after 10 incubation shots. In contrast, etching of p–Al_2O_3 was observed at 2 J/cm^2 after 5 shots, and only two incubation shots were needed before the onset of etching at 4, 5, or 6 J/cm^2 (Fig. 3, top). For sapphire, five incubation shots were required even at 6 J/cm^2 before significant etching occurred.

To better characterize the incubation phenomenon, we also carried out time–resolved measurements of ion currents in the plasma plume of material emitted from p-Al_2O_3, following relatively low-fluence KrF laser irradiation in vacuum. Figure 4 shows that the number of ions emitted from p–Al_2O_3 increases rapidly on successive laser shots at 1.1 J/cm^2, and saturates only after ~50 shots at 1.1 J/cm^2. The plume velocity, determined either from the leading edge or the peak of the ion probe current waveform, is in the range of 2–3 cm/μs (Fig. 5), corresponding to kinetic energies of 90–200 eV for species such as AlO. Interestingly, the plume velocity is much lower on the first several laser shots, but saturates at these high values after ~10 shots. This initial increase in plume velocity is consistent with the behavior shown in Fig. 3 (top), in that even p–Al_2O_3 apparently is damaged and made more energy–absorbing by successive laser shots at low fluence. Consequently, ions are accelerated to higher velocities by the expansion of the higher–density plasmas formed on successive laser shots at constant, low fluence.

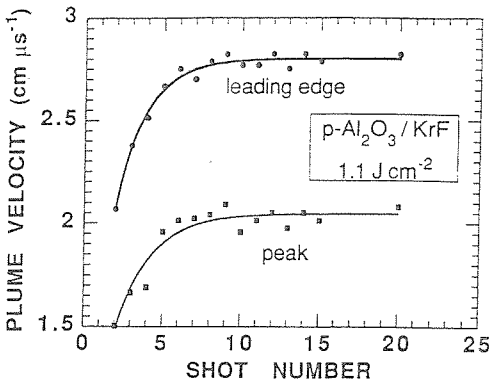

Figure 5. Plasma plume velocities vs laser shot number, inferred from the leading edge or peak of the ion probe signal (KrF laser, 1.1 J/cm^2, p–Al_2O_3).

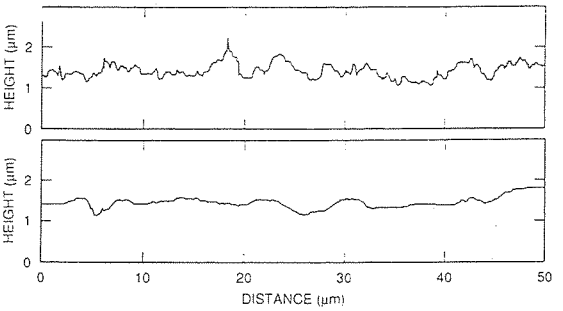

Figure 6. Atomic force microscope line-scan profiles for (top) as-received p–Al_2O_3 and (bottom) p–Al_2O_3 after 10 shots at 3 J/cm^2.

While studying the relationship between melting and the onset of laser etching (ablation that leaves a well-defined etch crater), we found that low laser fluences also produce significant changes in surface morphology, *even prior* to the onset of laser etching. Dektak profiles of the center of the laser-irradiated region on p-Al_2O_3, following 40 and 100 XeCl laser shots at 0.7 J/cm^2, close to the melting threshold, showed no laser-etched crater. On the contrary, the irradiated region was *raised up* and became *much rougher* than its surroundings. Thus, low-fluence XeCl radiation is strongly absorbed by p-Al_2O_3 and changes its morphology, but is not sufficiently intense to cause material removal that results in a crater. Similar behavior (roughening and elevation of the surface during incubation) has been reported for PLA of polymethyl methacrylate [11].

However, at higher fluences for which laser etching of p-Al_2O_3 does occur, we found significant *smoothing* of the p-Al_2O_3 surface within the laser–etched region. Figure 6 compares AFM line–scan profiles for p-Al_2O_3 in the as–received condition and after 10 XeCl shots at 3 J/cm^2. The profiles (as well as spatial-frequency transform spectra) clearly show that for repeated irradiation at 3 J/cm^2 the frequency distribution of surface height variation becomes much narrower, as rapid (high frequency) surface height variations are nearly eliminated. The amplitude of low-frequency surface height variations also decreases, and the bottom of the etched region becomes smoother than the original p-Al_2O_3 surface. The SEM images of Fig. 1 indicate that this occurs as adjacent polycrystalline grains are melted and coalesce, becoming continuously connected through molten flow. Thus, the principal effect of laser melting and solidification on the surface morphology of p-Al_2O_3, for fluences in the ablative–removal regime, is to remove the higher-frequency components of surface roughness, leaving only the gentle, longer-wavelength undulations in surface height.

DISCUSSION

The direct energy bandgap of sapphire is E_g ~9 eV, which is much larger than the energy $h\nu$ = 4.03 eV of a single 308-nm photon. The relatively easy etching of p-Al_2O_3 apparently results from strong energy absorption associated with the many polycrystalline grain boundaries (perhaps assisted by the low concentration of chemical impurities in p–Al_2O_3). The pronounced incubation behavior and higher E_d^{thresh} value for sapphire reflect the need to create a sufficient concentration of laser-generated absorption centers before efficient ablation and laser etching can occur.

It is interesting that once etching of sapphire occurs, its laser–etch rate with further irradiation is very similar to that of p–Al_2O_3, for E_d values well above both E_d^{thresh} values. For example, Fig. 3 shows that for E_d = 4, 5, and 6 J/cm^2 the first 10 shots *after* the incubation period produce etch depths of ~300 (~410), ~550 (~550), and ~700 (~660) nm for c-Al_2O_3 (p-Al_2O_3). The similarity of etch rates suggests that despite large differences in their initial morphology and in the number of incubation shots required for c– and p–Al_2O_3, these high-fluence shots ultimately produce similar damage morphologies and energy–absorption sites.

The most significant difference between our results for alumina and early studies of the mechanism for laser sputtering of sapphire is the evidence presented here that alumina undergoes melting and molten flow. In contrast, a non-thermal (primarily electronic) mechanism was suggested for sapphire [1–5]. However, it must be noted that our studies have focused on the high-fluence regime, in which many monolayers of material are ablated with each pulse. Under these conditions, the angular and velocity distributions of ablated species are drastically modified by the formation and expansion of a laser-generated plasma (Knudsen-layer formation) [16,17]. Coupling of laser energy to the target via the plasma (rather than by direct absorption) is expected to dominate after the first few nanoseconds of each pulse, under these high-fluence conditions. Our results reveal the importance of a "defect" absorption mechanism associated with grain boundaries that drastically reduces both the ablation threshold and the incubation period for alumina relative to sapphire, in agreement with the ideas of Dickinson et al [7,13]. However, our high-fluence results also reveal that grain boundaries cause a large difference in the ablation behavior of alumina and sapphire only on the first few shots, if E_d is well above both of their E_d^{thresh} values, so that these differences may disappear entirely in the very high-fluence regime ($>> 6$ J/cm^2).

ACKNOWLEDGEMENTS

We would like to acknowledge Thomas Thundat's assistance with atomic force microscopy. This research is sponsored by the Division of Materials Sciences, U.S. Department of Energy under contract DE-AC05-84OR21400 with Martin Marietta Energy Systems, Inc.

REFERENCES

1. J. E. Rothenburg and R. Kelly, *Nuc. Instr. and Methods in Physics Res.* **B1**, 291 (1984).
2. R. Kelly, J. J. Cuomo, P. A. Leary, J. E. Rothenburg, B. E. Braren, and C. F. Aliotta, *Nuc. Instr. and Methods in Physics Res.* **B9**, 329 (1985).
3. R. W. Dreyfus, R. Kelly, and R. E. Walkup, *Appl. Phys. Lett.* **49**, 1478 (1986).
4. R. W. Dreyfus, R. E. Walkup, and R. Kelly, *Radiation Effects* **99**, 199 (1986).
5. R. W. Dreyfus, F. A. McDonald, and R. J. von Gutfeld, *J. Vac. Sci. Technol.* **B5**, 1521 (1987).
6. M. A. Schildbach and A. V. Hamza, *Phys. Rev. B* **45**, 6197 (1992).
7. P. A. Eschbach, J. T. Dickinson, S. C. Langford, and L. R. Pederson, *J. Vac. Sci. and Technol. A* **7**, 2943 (1989).
8. S. C. Langford, L. C. Jensen, J. T. Dickinson, and L. R. Pederson, *J. Appl. Phys.* **68**, 4253 (1990).
9. S. Lazare and V. Grainer, *J. Appl. Phys.* **63**, 2110 (1988).
10. A. C. Tam, J. L. Brand, D. C. Cheng, and W. Zapka, *Appl. Phys. Lett.* **55**, 2045 (1989).
11. R. Srinivasan, B. Braren, and K. G. Casey, *J. Appl. Phys.* **68**, 1842 (1990).
12. S. Preuss, H.–C. Langowski, T. Damm, and M. Stuke, *Appl. Phys. A* **54**, 360 (1992).
13. J. T. Dickinson, S. C. Langford, L. C. Jensen, P. A. Eschbach, L. R. Pederson, and D. R. Baer, *J. Appl. Phys.* **68**, 1831 (1990).
14. J. T. Dickinson, S. C. Langford, and L. C. Jensen, in Laser Ablation: Mechanisms and Applications, ed. by J. C. Miller and R. F. Haglund, Jr. (Springer–Verlag, Berlin, 1991), p. 301.
15. J. T. Dickinson, S. C. Langford, and L. C. Jensen, in SPIE Vol. 1598: Lasers in Microelectronic Manufacturing, (SPIE–The Inter. Soc, for Optical Engin., Bellingham, WA, 1991), p. 72.
16. R. Kelly and R. W. Dreyfus, *Nuc. Instr. and Methods in Physics Res.* **B32**, 341 (1988).
17. R. Kelly, *J. Chem. Phys.* **92**, 5047 (1990).